Received: 19 September 2023 | Revised: 27 February 2024 | Accepted: 7 April 2024

DOI: 10.1002/nme.7490

RESEARCH ARTICLE

WILEY

Stabilization-free virtual element method for 2D elastoplastic problems

Bing-Bing Xu[1] | **Yi-Fan Wang**[2] | **Peter Wriggers**[1]

[1]Institute of Continuum Mechanics, Leibniz University Hannover, Garbsen, Germany

[2]School of Aeronautics and Astronautics, Dalian University of Technology, Dalian, China

Correspondence
Bing-Bing Xu, Institute of Continuum Mechanics, Leibniz University Hannover, Garbsen, Germany.
Email: bingbing.xu@ikm.uni-hannover.de

Abstract

In this paper, a novel first- and second-order stabilization-free virtual element method is proposed for two-dimensional elastoplastic problems. In contrast to traditional virtual element methods, the improved method does not require any stabilization, making the solution of nonlinear problems more reliable. The main idea is to modify the virtual element space to allow the computation of the higher-order L_2 projection operator, ensuring that the strain and stress represent the element energy accurately. Considering the flexibility of the stabilization-free virtual element method, the elastoplastic mechanical problems can be solved by radial return methods known from the traditional finite element framework. J_2 plasticity with hardening is considered for modeling the nonlinear response. Several numerical examples are provided to illustrate the capability and accuracy of the stabilization-free virtual element method.

KEYWORDS

nonlinear, plasticity, stabilization-free, virtual element method

1 | INTRODUCTION

Engineering problems are typically governed by a set of partial differential equations (PDEs) along with specified boundary conditions. In order to simulate and analyze the above problems, numerous numerical methods have been proposed, including finite element method (FEM), finite volume method (FVM), boundary element method (BEM), and meshless methods (MLMs). Among them, the finite element method is the most widely used in the field of computational solid mechanics and based on a sound mathematical framework. Standard finite element discretizations have limits when applied to complex geometries. Isogeometric analysis[1] is a technique that directly performs finite element calculations on complex geometric models. In addition, polygonal finite element is also a new technology needed to deal with complex geometric models.

Polygonal finite element methods have gained increasing attention due to their ability to allow more flexible computational domain discretizations. Some of the techniques can be listed as Polygonal Finite Element Method (PFEM),[2,3] discontinuous Galerkin methods (DG),[4,5] mimetic finite difference methods (MFD),[6–8] and some other methods like the extended FEMs (XFEM)[9] and generalised FEMs (GFEM).[10] The scaled boundary finite element method (SBFEM)[11–13]

This contribution is dedicated to Robert L. Taylor in honor of his 90th birthday and his enduring accomplishments in computational mechanics, finite element technology, and the associated software, FEAP. The third author had the privilege witnessing Bob's dedication, passion, and commitment to education and research and would like to express gratitude for his unwavering support and friendship spanning over four decades. The choice of the topic for our contribution is influenced by the fact that Bob Taylor is currently engaged in the same field.

is another special type of polygonal finite element methods, which significantly differs from the above polygonal finite element methods in the process of constructing variational schemes.

In the past decade, the virtual element method proposed in References 14,15 has received increasing attention due to its ability to handle polygon or polyhedral elements of convex and non-convex shape. The virtual element method does not require the construction of interpolation functions (shape functions) for polygonal (polyhedral) elements and also avoids complex domain integration in the element.[16] Due to these characteristics, the virtual element method has strong advantages in dealing with hanging node elements, crack growth problems[17,18] and adaptive mesh refinement.[19] Despite its short history beginning in 2013, the VEM has been developed for the linear elastic problems,[16,20–23] hyperelastic materials at finite deformations,[24–27] contact problems,[28–31] elastodynamics problems,[32–35] finite elastoplastic deformations,[36–38] phase field modeling problems[39,40] and for eigenvalue problems.[41,42]

In the VEM, the variable u is replaced by its projection Πu onto a polynomial space. As a result, the stiffness matrix becomes rank-deficient and a stabilization term is required to avoid the development of the zero-energy hourglass modes. Some stabilization techniques have been proposed for linear and nonlinear problems.[14,24,25,43] However, the presence of stabilization terms requires the introduction of stability parameters which eventually can bias the approximate solution. Therefore, it is desirable to construct a new VEM formulation that does not require any stabilization term. An enhanced VEM formulation was proposed in Reference 44 that can bypass the need for stabilization terms for the first-order VEM ($k = 1$). Besides, a self-stabilized virtual element formulation was proposed by Andrea[43] for 2D 4-node elements based on the Hu-Washizu variational approach. Recently in References 45,46, a first-order stabilization-free virtual element method (SFVEM) was introduced for the Poisson equation. The basic idea is to modify the first-order virtual element space to allow the computation of a higher-order L_2 projection of the gradient.[47] The well-posedness was proven in References 45,48 and the discrete problem can be solved without a stabilizing bilinear form. According to these developments, the stabilization-free virtual element method has been extended to the Laplacian eigenvalue problem,[49] linear plane elasticity in References 47,50, and 3D elasticity in Reference 51. All the above contributions are considered linear problems. Since stabilization terms are not required for the stabilization-free formulation, an extension of the method to the fields of nonlinear problems is advantageous. Before this, the author tried to apply this stabilization-free format to two-dimensional hyperelasticity problems.[52]

In addition to the problem of hyperelasticity, classical small-strain elastoplasticity is of special significance as it finds extensive application in engineering analysis and represents an important topic in the nonlinear continuum mechanics of solids. In essence, elastoplastic problems can be characterized by quasistatic models with various yield criteria, flow rules or internal variables. Considering the ability of the virtual element method to handle complex problems, the stabilization-free virtual element method (SFVEM) combined with the radial-return mapping algorithm will be developed for elastoplastic analysis. Considering the complexity of the elastoplastic problem, we only consider the simpler elastoplastic constitutive model in this work.

In this paper, we provide a computational framework of SFVEM for 2D elastoplastic problems, including the calculation of the high-order L_2 projection matrix $\mathbf{\Pi}^m$ for $k = 1, 2$ and the associated approximate expressions for gradients. The framework does not require any stabilization terms and can be extended to other nonlinear problems. For small-strain elastoplastic, the Newton-Raphson (N-R) method will be used with the following standard computational procedure

(1) implicit time-discretization of the plastic evolution equation;
(2) space discretization by the stabilization-free virtual element method;
(3) solution of a resulting discretized system by the Newton method.

The paper is organized as follows. The necessary theoretical basis for elastoplastic problems is summarized in Section 2. The basic principles of the stabilization-free virtual element method and the calculation of different projection operators are given in Section 3. Next, the stabilization-free virtual element formulation for the elastoplastic problem is provided in Section 4. Some numerical examples are presented and discussed in Section 5. Finally, the paper closes with some concluding remarks in Section 6.

2 | PROBLEM FORMULATION

In this section, we consider an elastoplastic body occupying a bounded domain $\Omega \in \mathbb{R}^2$ with boundary $\Gamma = \partial\Omega = \Gamma_D \cup \Gamma_N$ and $\Gamma_D \cap \Gamma_N = \emptyset$. Γ_D is the Dirichlet boundary for prescribed displacements $\boldsymbol{u}_D \in \mathcal{H}^1(\Omega; \mathbb{R}^2)$, Γ_N is the Neumann

boundary for prescribed tractions $\boldsymbol{f}_T \in \mathcal{L}^2(\Gamma_N; \mathbb{R}^2)$. At any point $\boldsymbol{x} \in \Omega$, the total strain can be decomposed into elastic $\boldsymbol{\varepsilon}^e$ and plastic parts $\boldsymbol{\varepsilon}^e$ when only small strains are present

$$\boldsymbol{\varepsilon} = \boldsymbol{\varepsilon}^e + \boldsymbol{\varepsilon}^p. \tag{1}$$

A free energy per unit of volume[53] can be defined as

$$\mathcal{W}(\boldsymbol{\varepsilon}^e, \boldsymbol{\alpha}) = \mathcal{W}_e(\boldsymbol{\varepsilon}^e) + \mathcal{W}_v(\boldsymbol{\alpha}), \tag{2}$$

where $\mathcal{W}_e(\boldsymbol{\varepsilon}^e)$ is elastic strain energy function and $\mathcal{W}_v(\boldsymbol{\alpha})$ is a potential function (plastic potential energy) for the hardening variables $\boldsymbol{\alpha}$. The partial derivative of $\mathcal{W}$ yields

$$\boldsymbol{\sigma} = \frac{\partial \mathcal{W}(\boldsymbol{\varepsilon}^e, \boldsymbol{\alpha})}{\partial \boldsymbol{\varepsilon}^e}, \quad \boldsymbol{q} = -\frac{\partial \mathcal{W}(\boldsymbol{\varepsilon}^e, \boldsymbol{\alpha})}{\partial \boldsymbol{\alpha}}, \tag{3}$$

where $\boldsymbol{\sigma}$ is the stress and $\boldsymbol{q}$ is the back stress. Then, we defined volumetric and deviatoric parts of strain and stress

$$\boldsymbol{e} = \boldsymbol{\varepsilon} - \frac{1}{3}\mathrm{tr}(\boldsymbol{\varepsilon})\boldsymbol{I}, \quad \varepsilon_V = \frac{1}{3}\mathrm{tr}(\boldsymbol{\varepsilon}), \tag{4}$$

$$\boldsymbol{s} = \boldsymbol{\sigma} - \frac{1}{3}\mathrm{tr}(\boldsymbol{\sigma})\boldsymbol{I}, \quad p = \frac{1}{3}\mathrm{tr}(\boldsymbol{\sigma}), \tag{5}$$

where $\boldsymbol{I} \in \mathbb{R}^{2\times 2}$ is the second order unit tensor.

For small strains, the elastic strain energy function has the form as

$$\mathcal{W}_e = \frac{1}{2}\boldsymbol{\varepsilon}^e : \boldsymbol{C} : \boldsymbol{\varepsilon}^e. \tag{6}$$

where $\boldsymbol{C}$ denotes the fourth-order elastic tensor which has the form as

$$\boldsymbol{C} = K\boldsymbol{I} \otimes \boldsymbol{I} + 2\mu \boldsymbol{I}_{\mathrm{dev}}, \tag{7}$$

where the parameters K and μ are the elastic bulk and shear moduli, respectively, $\boldsymbol{I}_{\mathrm{dev}}$ is defined as $\boldsymbol{I}_{\mathrm{dev}} = \boldsymbol{I}_4 - \frac{1}{3}\boldsymbol{I} \otimes \boldsymbol{I}$, $\boldsymbol{I}_4$ is the fourth-order tensor which can be written as

$$(\boldsymbol{I}_4)_{ijkl} = \frac{1}{2}(\delta_{ik}\delta_{jl} + \delta_{il}\delta_{jk}). \tag{8}$$

Besides, the plastic potential energy can be written as

$$\mathcal{W}_v = \frac{1}{2}\hat{H}\hat{\alpha}^2 + \frac{1}{3}H||\boldsymbol{\alpha}||^2, \tag{9}$$

where $\hat{\alpha}$ and $\boldsymbol{\alpha}$ are the isotropic and kinematic hardening variables, respectively. Substituting Equations (9) into (3), we have

$$\boldsymbol{q} = -\frac{2}{3}H\boldsymbol{\alpha}, \quad \hat{q} = -\hat{H}\hat{\alpha}. \tag{10}$$

For linear isotropic and kinematic hardening, the yield function is given by

$$f(\boldsymbol{s}, \boldsymbol{q}, \hat{q}) = ||\boldsymbol{s} - \boldsymbol{q}|| - \sqrt{\frac{2}{3}}(\sigma_Y^0 - \hat{q}) \leq 0, \tag{11}$$

where σ_Y^0 is the initial yield stress, $\boldsymbol{s}$ is the deviatoric stress tensor and $\boldsymbol{s} = 2\mu\boldsymbol{e}$, $\boldsymbol{\eta} = \boldsymbol{s} - \boldsymbol{q}$ is the shifted stress, $||\boldsymbol{\eta}|| = \sqrt{\boldsymbol{\eta} : \boldsymbol{\eta}}$.

For associative J_2 plasticity, we have

$$\dot{\boldsymbol{e}}^p = \lambda \frac{\partial f}{\partial \boldsymbol{s}}, \quad \dot{\boldsymbol{\alpha}} = \lambda \frac{\partial f}{\partial \boldsymbol{q}}, \quad \dot{\hat{\alpha}} = \lambda \frac{\partial f}{\partial \hat{q}}, \tag{12}$$

where λ is a scalar that determines the size of the plastic strain increment. Using the flow condition (11), the derivative of f yields

$$\frac{\partial f}{\partial \boldsymbol{s}} = \frac{\boldsymbol{s}-\boldsymbol{q}}{||\boldsymbol{s}-\boldsymbol{q}||} = \frac{\boldsymbol{\eta}}{||\boldsymbol{\eta}||} =: \boldsymbol{N}, \frac{\partial f}{\partial \boldsymbol{q}} = -\boldsymbol{N}. \tag{13}$$

Then the evolution equations become

$$\dot{\boldsymbol{e}}^p = \lambda \boldsymbol{N}, \quad \dot{\boldsymbol{\alpha}} = -\lambda \boldsymbol{N}, \quad \dot{\hat{\alpha}} = \lambda \sqrt{\frac{2}{3}}. \tag{14}$$

The Karush-Kuhn-Tucker (KKT) condition reads as

$$\lambda \geqslant 0, \quad f \leqslant 0, \quad \lambda f = 0. \tag{15}$$

3 | STABILIZATION-FREE VIRTUAL ELEMENT METHOD

3.1 | Mesh assumptions and polynomial basis

Let $\mathcal{T}_h$ be a family of partitions of the domain Ω into a set of non-overlapping arbitrary polygonal elements, $\mathcal{E}_h$ be the set of edges e of $\mathcal{T}_h$. For each element $E \in \mathcal{T}_h$ with n_E edges, the diameter is h_E and the area is $|E|$. We assume that $\mathcal{T}_h$ satisfies the mesh assumptions for VEM[54] such that

- every polygonal element $E \in \mathcal{T}_h$ is star-shaped with respect to a ball of radius $\geqslant Ch_E$;
- every edge $e \in \partial E$ with the length h_e satisfies $h_e > Ch_E$,

where C is a suitable positive constant. It should be noted that different from FEM, VEM allows for strongly distorted elements since no geometry mapping is required. Some typical polygonal elements are shown in Figure 1.

Let $\mathbb{P}_k(E)$ be the function space on E that consists of all polynomials of order $\leq k$. The dimension of the function space is

$$N_P := \dim(\mathbb{P}_k(E)) = \frac{(k+1)(k+2)}{2}. \tag{16}$$

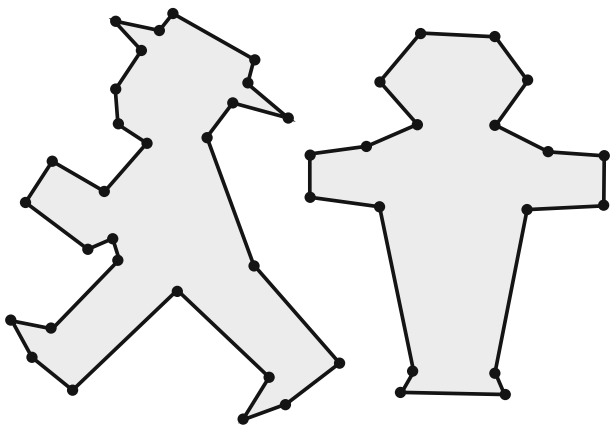

FIGURE 1 First order polygonal element used in VEM.

Then we can define the set of scaled monomials $\mathcal{M}_k(E)$ of degree equal to N_P as

$$\mathcal{M}_k(E) := \left\{ \left(\frac{\boldsymbol{x} - \boldsymbol{x}_E}{h_E} \right)^{\boldsymbol{s}}, |\boldsymbol{s}| \leq k \right\}, \tag{17}$$

where $\boldsymbol{x}_E$ are the cartesian coordinates of the centroid of E, $|\boldsymbol{s}| := s_1 + s_2$ and $\boldsymbol{x}^{\boldsymbol{s}} := x_1^{s_1} x_2^{s_2}$. Besides, we still define the set of scaled monomials $\mathcal{M}_k^*(E)$ as

$$\mathcal{M}_k^*(E) := \left\{ \left(\frac{\boldsymbol{x} - \boldsymbol{x}_E}{h_E} \right)^{\boldsymbol{s}}, |\boldsymbol{s}| = k \right\}. \tag{18}$$

Should be mentioned that the scaled monomials are used as the basis for $\mathbb{P}_k(E)$ to ensure all degrees of freedom scale like 1 concerning the element size h_E.[55] Besides, $\mathcal{M}_k(E)$ is the basis for $\mathbb{P}_k(E)$, m_α is used to refer to an element of $\mathcal{M}_k(E)$. The scaled monomials set $\mathcal{M}_k(E)$ is used in the virtual element method for scalar as well as vector problems.

3.2 | Virtual element space and $\mathcal{H}_1$ projection operator

The virtual element space can be defined as

$$\mathcal{V}_k(E) := \left\{ u_h \in H^1(E) : \Delta u \in \mathbb{P}_{k-2}(E), u|_{\partial E} = \mathbb{B}_k(\partial E) \right\}, \tag{19}$$

where $\mathbb{P}_k$ is a polynomial with the highest order not exceeding k,

$$\mathbb{B}_k(\partial E) := \{ u_h \in C(\partial E) : u_e \in \mathbb{P}_k(e), e \subset \partial E \}. \tag{20}$$

In $\mathcal{V}_k(E)$, the degrees of freedom are selected as

- the values of u_h at the vertices;
- the values of u_h at $k-1$ uniformly spaced points on each edge e;
- for $k > 1$, the moments

$$\frac{1}{|E|} \int_E u_h m_\alpha \mathrm{d}\Omega, \quad \forall m_\alpha \in \mathcal{M}_{k-2}(E).$$

Easy to find that $\mathbb{B}_k(\partial E)$ is a linear space of dimension $n_E + n_E(k-1) = n_E k$. Since a polynomial of order k requires $(k+1)(k+2)/2$ parameters and $m_\alpha \in \mathcal{M}_{k-2}(E)$ for the internal degrees of freedom, there are another $k(k-1)/2$ parameters to describe a polygonal of order $k-2$ in the element. Then the dimension of $\mathcal{V}_k(E)$ can be obtained as

$$\begin{aligned} N_E &:= \dim(\mathcal{V}_k(E)) \\ &= n_E + n_E(k-1) + \frac{k(k-1)}{2} = n_E k + \frac{k(k-1)}{2} \end{aligned} \tag{21}$$

where n_E is the number of edges, the last term of Equation (21) corresponds to the dimension of polynomials of degree $\leq k-2$ in two dimensions ($\Delta u \in \mathbb{P}_{k-2}(E)$).

The projection operator is selected as the projector $\Pi_k^\nabla(E)$, which is defined as

$$\Pi_k^\nabla(E) : \mathcal{V}_k(E) \to \mathbb{P}_k(E), u_h \mapsto \Pi_k^\nabla u, \tag{22}$$

and the projection Π_k^∇ defined for $u_h \in \mathcal{V}_k(E)$ can be calculated by the orthogonality condition,

$$\int_E \nabla \Pi_k^\nabla u_h \cdot \nabla p \, \mathrm{d}\Omega = \int_E \nabla u_h \cdot \nabla p \, \mathrm{d}\Omega, \tag{23}$$

where $\forall u_h \in \mathcal{V}_k(E)$, $\forall p \in \mathbb{P}_k(E)$. In order to define Π_k^∇ uniquely, we should add the following constraints

$$P_0\left(\Pi_k^\nabla u_h - u_h\right) = 0. \tag{24}$$

A suitable choice of constraint is

$$P_0(u_h) := \frac{1}{|E|}\int_E u_h \mathrm{d}\Omega. \tag{25}$$

Note that this projection in (23) is different from Reference 47 where the elastic energy enters the projection. Here, for the nonlinear case, we only project the gradient, this obtains a formulation that is valid for any constitutive model.

Considering the Green formula, Equation (23) can be deduced as

$$\int_E \nabla\Pi_k^\nabla u_h \cdot \nabla p \ \mathrm{d}\Omega = -\int_E u_h \cdot \Delta p \ \mathrm{d}\Omega + \int_{\partial E} u_h \cdot \frac{\partial p}{\partial \boldsymbol{n}}\mathrm{d}\Gamma. \tag{26}$$

To solve Equation (26), we can expand the projection operator Π_k^∇ in different bases $\forall m_\alpha \in \mathcal{M}_k, \forall \phi_j \in \mathcal{V}_k$ as

$$\Pi_k^\nabla \phi_i = \sum_{\alpha=1}^{N_P} a_{\alpha,i} m_\alpha = \sum_{j=1}^{N_E} s_{j,i}\phi_j, \tag{27}$$

where $N_P := \dim(\mathcal{M}_k)$. Equation (27) can be written in the following matrix form

$$\Pi_k^\nabla \boldsymbol{\phi}^T = \boldsymbol{m}^T \boldsymbol{\Pi}_{k*}^\nabla = \boldsymbol{\phi}^T \boldsymbol{\Pi}_k^\nabla. \tag{28}$$

Substituting Equations (28) into (26), we obtain

$$\int_E \nabla \boldsymbol{m} \cdot \nabla\Pi_k^\nabla \boldsymbol{\phi}^T \ \mathrm{d}\Omega = -\int_E \Delta \boldsymbol{m} \cdot \boldsymbol{\phi}^T \ \mathrm{d}\Omega + \int_{\partial E} (\nabla \boldsymbol{m} \cdot \boldsymbol{n})\boldsymbol{\phi}^T \mathrm{d}\Gamma. \tag{29}$$

We can define a matrix $\boldsymbol{D}$ with

$$(\boldsymbol{D})_{j,\alpha} = \mathrm{dof}_j(m_\alpha) \tag{30}$$

for re-expressing polynomials in terms of the basis of $\mathcal{V}_k(E)$, then we have

$$\boldsymbol{m}^T = \boldsymbol{\phi}^T \boldsymbol{D}, \quad \boldsymbol{\Pi}_k^\nabla = \boldsymbol{D}\boldsymbol{\Pi}_{k*}^\nabla. \tag{31}$$

With Equations (28) and (31), Equation (29) can be re-formulated as

$$\int_E \nabla \boldsymbol{m} \cdot \nabla \boldsymbol{m}^T \mathrm{d}\Omega \boldsymbol{\Pi}_{k*}^\nabla = -\int_E \Delta \boldsymbol{m} \cdot \boldsymbol{\phi}^T \ \mathrm{d}\Omega + \int_{\partial E} (\nabla \boldsymbol{m} \cdot \boldsymbol{n})\boldsymbol{\phi}^T \mathrm{d}\Gamma, \tag{32}$$

which then leads to the matrix form

$$\boldsymbol{G}^\nabla \boldsymbol{\Pi}_{k*}^\nabla = \boldsymbol{B}^\nabla, \tag{33}$$

where the size of $\boldsymbol{G}^\nabla$ is $N_P \times N_P$ and the size of $\boldsymbol{B}^\nabla$ is $N_E \times N_P$. The constraint condition should be considered during the calculation of $\boldsymbol{B}$ and $\boldsymbol{G}$. Given the definition of degree of freedom, it is possible to compute matrix $\boldsymbol{B}^\nabla$. It should be mentioned that it is not necessary to calculate matrix $\boldsymbol{G}^\nabla$ because $\boldsymbol{G}^\nabla = \boldsymbol{D}\boldsymbol{B}^\nabla$.

3.3 | L_2 projection operator

The core idea of VEM is to use local approximation spaces whose functions are solutions to suitable differential problems. Besides, a suitable stabilization term should be added since the projection Π_{k*}^∇ does not lead to an element matrix with

full rank. For elastoplastic problems, the computation of the projection operators and the construction of stabilization terms is complex and problem-depending. In this work, a stabilization-free VEM is proposed and extended for use in elastoplastic problems.

To obtain the discrete bilinear form for the stabilization-free VEM, we define the L_2 projection operator $\Pi^0_{k,E}$ of the variable field and $\mathbf{\Pi}^0_{l,E}\nabla$ of the gradient of the variable field, which is defined as

$$\Pi^0_{k,E} : \mathcal{H}^1(E) \to \mathbb{P}_k(E), \tag{34}$$

$$\mathbf{\Pi}^0_{l,E}\nabla : \mathcal{H}^1(E) \to \left[\mathbb{P}_l(E)\right]^2, \tag{35}$$

where $l \in \mathbb{N}$ is a parameter defining the order of the necessary polynomial space for sufficient stabilization which depends on the order k and the number of edges n_E. As given in Reference 48, the relationship

$$(k+l)(k+l+1) \geq kn_E + k(k+1) - 3 \tag{36}$$

holds. Another relationship for the elastic problem is formulated based on an eigenvalue analysis[50,52] with

$$n_E \leq 2l - 2k + 5. \tag{37}$$

By representing the virtual variable field u and the approximated gradient ∇u in terms of the basis functions, we can write

$$u \approx u_h = \boldsymbol{\phi}^T \tilde{\boldsymbol{u}}, \tag{38}$$

$$\nabla u \approx \nabla u_h = (\boldsymbol{N}^p)^T \tilde{\epsilon}, \tag{39}$$

where $\widetilde{\square}$ represents a vector; $\boldsymbol{\phi}$ is a vector of the basis function in $\mathcal{V}_k(E)$ and the length is N_E; $\tilde{\boldsymbol{u}} \in \mathbb{R}^{N_E}$; $\epsilon := \nabla u_h$,and $\boldsymbol{N}^p$ is a matrix (size $l(l+1) \times 2$) which contains the polynomial basis

$$\begin{aligned}\left(\boldsymbol{N}^p\right)^T &:= \begin{bmatrix} 1 & \xi & \eta & \cdots & \eta^l & 0 & 0 & 0 & \cdots & 0 \\ 0 & 0 & 0 & \cdots & 0 & 1 & \xi & \eta & \cdots & \eta^l \end{bmatrix}^T \\ &= \begin{bmatrix} \boldsymbol{m}_l^T & \boldsymbol{0}^T \\ \boldsymbol{0}^T & \boldsymbol{m}_l^T \end{bmatrix}.\end{aligned} \tag{40}$$

In order to solve the L_2 projection operator for variable gradients $\mathbf{\Pi}^0_{l,E}\nabla$, we let $u_h \in \mathcal{H}^1(E)$ satisfy the following orthogonality condition

$$\int_E \boldsymbol{p}^T \mathbf{\Pi}^0_{l,E} \nabla u_h \, \mathrm{d}\Omega = \int_E \boldsymbol{p}^T \nabla u_h \, \mathrm{d}\Omega, \tag{41}$$

where $\boldsymbol{p} \in [\mathbb{P}_l]^2$. Considering using integrals by parts and Gaussian divergence theorem, the right side of Equation (41) becomes

$$\int_E \boldsymbol{p}^T \nabla u_h \, \mathrm{d}\Omega = \int_{\partial E} \left(\boldsymbol{p}^T \boldsymbol{n}\right) u_h \mathrm{d}\Gamma - \int_E (\mathrm{div}\boldsymbol{p}) u_h \, \mathrm{d}\Omega, \tag{42}$$

where $\boldsymbol{n}$ is the edge normal vector. Substituting Equations (42) into (41), yields

$$\int_E \boldsymbol{p}^T \mathbf{\Pi}^0_{l,E} \nabla u_h \, \mathrm{d}\Omega = \int_{\partial E} \left(\boldsymbol{p}^T \cdot \boldsymbol{n}\right) u_h \mathrm{d}\Gamma - \int_E (\mathrm{div}\boldsymbol{p}) u_h \, \mathrm{d}\Omega, \quad \forall \boldsymbol{p} \in [\mathcal{P}_l(E)]^2. \tag{43}$$

As given in Reference 16, we denote by $\mathbf{\Pi}^m$ the operator $\mathbf{\Pi}^0_{l,E}\nabla$ expressed as a matrix, thus the projected gradient results in

$$\mathbf{\Pi}^0_{l,E}\nabla u = \left(\boldsymbol{N}^p\right)^T \mathbf{\Pi}^m \tilde{\boldsymbol{u}}. \tag{44}$$

Similar to the gradient of variable, we can expand $\boldsymbol{p}$ in terms of polygonal basis in $[\mathbb{P}_l]^2$ as

$$\boldsymbol{p} = \left(\boldsymbol{N}^p\right)^T \tilde{\boldsymbol{p}}. \tag{45}$$

Substituting Equations (44) and (45) into (43), lead to

$$\tilde{\boldsymbol{p}}^T \int_E \boldsymbol{N}^p \left(\boldsymbol{N}^p\right)^T \mathrm{d}\Omega \boldsymbol{\Pi}^m \tilde{\boldsymbol{u}} = \tilde{\boldsymbol{p}}^T \int_{\partial E} \left(\boldsymbol{N}^p \cdot \boldsymbol{n}\right) \boldsymbol{\phi}^T \mathrm{d}\Gamma \tilde{\boldsymbol{u}} - \tilde{\boldsymbol{p}}^T \int_E \left(\mathrm{div}\boldsymbol{N}^p\right) \boldsymbol{\phi}^T \mathrm{d}\Omega \tilde{\boldsymbol{u}}. \tag{46}$$

Since this is true for all $\tilde{\boldsymbol{u}}$ and $\tilde{\boldsymbol{p}}$, the above Equation (46) can be written as

$$\int_E \boldsymbol{N}^p \left(\boldsymbol{N}^p\right)^T \mathrm{d}\Omega \boldsymbol{\Pi}^m = \int_{\partial E} \left(\boldsymbol{N}^p \cdot \boldsymbol{n}\right) \boldsymbol{\phi}^T \mathrm{d}\Gamma - \int_E \left(\mathrm{div}\boldsymbol{N}^p\right) \boldsymbol{\phi}^T \mathrm{d}\Omega. \tag{47}$$

If the right side of Equation (47) is computable, then the projection matrix $\boldsymbol{\Pi}^m$ can be calculated by

$$\boldsymbol{\Pi}^m = \boldsymbol{G}^{-1} \boldsymbol{B}, \tag{48}$$

where

$$\boldsymbol{G} := \int_E \boldsymbol{N}^p \left(\boldsymbol{N}^p\right)^T \mathrm{d}\Omega, \tag{49}$$

$$\boldsymbol{B} := \int_{\partial E} \left(\boldsymbol{N}^p \cdot \boldsymbol{n}\right) \boldsymbol{\phi}^T \mathrm{d}\Gamma - \int_E \left(\mathrm{div}\boldsymbol{N}^p\right) \boldsymbol{\phi}^T \mathrm{d}\Omega. \tag{50}$$

For matrix $\boldsymbol{G}$, we only need to determine integrals of the form

$$\int_E \xi^p \eta^q \mathrm{d}\Omega \quad \text{for} \quad 0 \le p + q \le 2l \tag{51}$$

which can be calculated by partitioning E into a set of triangles $\mathcal{T}_n$ (as shown in Figure 2) and adopting a Gauss quadrature rule.

Compared with Equation (33), the calculation of matrix $\boldsymbol{B}$ reveals the major difference between the proposed stabilization-free VEM and the conventional VEM. This calculation is based on the following definitions

$$\boldsymbol{I}_1 := \int_{\partial E} \left(\boldsymbol{N}^p \cdot \boldsymbol{n}\right) \boldsymbol{\phi}^T \mathrm{d}\Gamma, \tag{52}$$

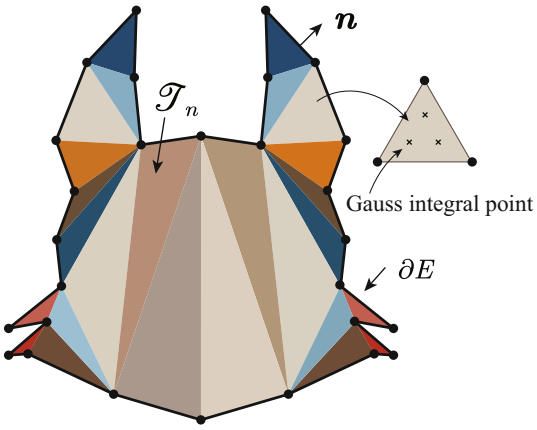

FIGURE 2 Triangulation of polygonal element.

$$\boldsymbol{I}_2 := \int_E \left(\mathrm{div}\boldsymbol{N}^p\right)\boldsymbol{\phi}^T \mathrm{d}\Omega. \tag{53}$$

The basis function $\boldsymbol{\phi}$ is known at the polygonal boundary of the element $\partial\Omega_E$ which can be described by a polynomial of degree k. Thus the term $\boldsymbol{I}_1$ can be calculated by the one-dimensional Gaussian integral as

$$\boldsymbol{I}_1 = \sum_{e\in\partial E}\int_e \boldsymbol{N}^p\boldsymbol{n}\boldsymbol{\phi}^T \mathrm{d}\Gamma = \sum_{e\in\partial E}\frac{|e|}{2}\int_{-1}^{1}\boldsymbol{N}^p\boldsymbol{n}\boldsymbol{\phi}^T \mathrm{d}s. \tag{54}$$

Next is the calculation of $\boldsymbol{I}_2$. To do this, let us revisit the definition of L_2 projection for scalar given in Equation (34), then we have the following orthogonality condition

$$\int_E \Pi^0_{k,E}u_h p \ \mathrm{d}\Omega = \int_E u_h p \ \mathrm{d}\Omega, \forall u_h \in \mathcal{V}_k(E), \forall p \in \mathbb{P}_k(E). \tag{55}$$

Considering the basis $\boldsymbol{\phi}$ and $\boldsymbol{m} \in \mathcal{M}_k$ for function space $\mathcal{V}_k(E)$ and $\mathbb{P}_k(E)$, Equation (55) can be written as

$$\int_E \boldsymbol{m}\Pi^0_{k,E}\boldsymbol{\phi}^T \mathrm{d}\Omega = \int_E \boldsymbol{m}\boldsymbol{\phi}^T \mathrm{d}\Omega. \tag{56}$$

Similar to the traditional VEM, we can defining the $\boldsymbol{\Pi}^0_{k*}$ to be the matrix of $\Pi^0_{k,E}$ on the basis of $\boldsymbol{m}$ and $\boldsymbol{\Pi}^0_k$ being related to the basis of $\boldsymbol{\phi}^T$

$$\Pi^0_{k,E}\boldsymbol{\phi}^T = \boldsymbol{\phi}^T\boldsymbol{\Pi}^0_k = \boldsymbol{m}^T\boldsymbol{\Pi}^0_{k*}, \tag{57}$$

then Equation (56) becomes

$$\int_E \boldsymbol{m}\boldsymbol{m}^T \mathrm{d}\Omega\boldsymbol{\Pi}^0_{k*} = \int_E \boldsymbol{m}\boldsymbol{\phi}^T \mathrm{d}\Omega, \tag{58}$$

or in the matrix form

$$\boldsymbol{H}\boldsymbol{\Pi}^0_{k*} = \boldsymbol{\Phi}, \tag{59}$$

where

$$\boldsymbol{H} := \int_E \boldsymbol{m}\boldsymbol{m}^T \mathrm{d}\Omega, \tag{60}$$

$$\boldsymbol{\Phi} := \int_E \boldsymbol{m}\boldsymbol{\phi}^T \mathrm{d}\Omega. \tag{61}$$

By using the triangular partition the matrix $\boldsymbol{H}$ can be calculated numerically. Once we compute the matrix $\boldsymbol{\Phi}$, we can further calculate the L_2 projection matrix $\boldsymbol{\Pi}^0_{k*}$, thereby calculating $\boldsymbol{I}_2$ and the L_2 projection matrix $\boldsymbol{\Pi}^m$. The relationship is given as

$$\boldsymbol{I}_2 = \int_E \left(\mathrm{div}\boldsymbol{N}^p\right)\boldsymbol{\phi}^T \mathrm{d}\Omega = \int_E \left(\mathrm{div}\boldsymbol{N}^p\right)\boldsymbol{\phi}^T\boldsymbol{\Pi}^0_k \mathrm{d}\Omega = \int_E \left(\mathrm{div}\boldsymbol{N}^p\right)\boldsymbol{m}_k^T \mathrm{d}\Omega\boldsymbol{\Pi}^0_{k*}, \tag{62}$$

and

$$\boldsymbol{B} = \boldsymbol{I}_1 - \boldsymbol{I}_2. \tag{63}$$

The basis function $\boldsymbol{\phi}$ is not explicitly known inside the polygonal virtual element. In traditional VEM, the integral terms within the element can be eliminated using the definition of degrees of freedom. This also means that the matrix $\boldsymbol{\Phi}$ in Equation (61) as well as the matrix $\boldsymbol{B}$ in Equation (50) is not computable in the current function space.

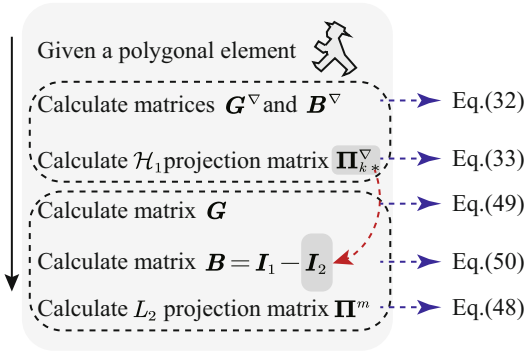

FIGURE 3 Flowchart for calculating the L_2 projection matrix Π^m for $k = 1$ and $k = 2$.

However, we can consider the following enlarged enhanced virtual element space[56]

$$\tilde{\mathcal{V}}_k(E) := \left\{ v \in \mathcal{H}^1(E) : v|_{\partial E} \in \mathbb{B}_k(\partial E), \Delta v \in \mathbb{P}_k(E) \right\}. \tag{64}$$

and we obtain

$$\int_E \Pi^0_k v p \, \mathrm{d}\Omega = \int_E \Pi^{\nabla}_k v p \, \mathrm{d}\Omega, \quad \forall p \in \mathcal{M}^*_{k-1} \cup \mathcal{M}^*_k. \tag{65}$$

As demonstrated in Reference 56, for $k = 1$ and $k = 2$, we deduct

$$\mathbf{\Pi}^0_k = \mathbf{\Pi}^{\nabla}_k, \quad \mathbf{\Pi}^0_{k*} = \mathbf{\Pi}^{\nabla}_{k*}, \quad \mathbf{\Pi}^0_k = \boldsymbol{D}\mathbf{\Pi}^0_{k*} \tag{66}$$

In this work, only the first and second-order VEM ($k = 1$ and $k = 2$) is used for the elastoplastic problem. Thus Equation (66) can be used and the L_2 projection can be computed lastly. Using the relationship given in Equation (66), the matrix $\boldsymbol{I}_2$ follows as

$$\boldsymbol{I}_2 = \int_E \left(\mathrm{div}\boldsymbol{N}^p\right) \boldsymbol{m}_k^T \mathrm{d}\Omega \mathbf{\Pi}^{\nabla}_{k*}, \tag{67}$$

where $\mathbf{\Pi}^{\nabla}_{k*}$ is the H_1 projection (Ritz projection) matrix given in Equation (33). Substituting Equations (67) into (63) yields the L_2 projection matrix $\mathbf{\Pi}^m$.

The flowchart for calculating the L_2 projection matrix $\mathbf{\Pi}^m$ for $k = 1$ and $k = 2$ is provided in Figure 3. Once the L_2 projection matrix $\mathbf{\Pi}^m$ is obtained, we can directly approximate the gradient of the variable, which is expressed as

$$\nabla u \approx \mathbf{\Pi}^0_{l,E} \nabla u = \left(\boldsymbol{N}^p\right)^T \mathbf{\Pi}^m \tilde{\boldsymbol{u}}, \tag{68}$$

where $\boldsymbol{N}_p$ is given in Equation (40), u is any scalar field.

4 | STABILIZATION-FREE VIRTUAL ELEMENT FORMULATION FOR ELASTOPLASTIC PROBLEM

The main objective of this work is to extend the stabilization-free VEM (SFVEM) to elastoplastic problems. In Section 3, we have deduced the matrix form of the L_2 projection operator for the gradient of any scalar field u (as well as v). In this paper, we use the scalar field gradient approximation to construct the vector field gradient approximation directly.

4.1 | Tangent stiffness matrix

When dealing with elastoplastic problems applying the return-mapping algorithm, one has to compute the total strain from the equilibrium equation and then use the elastic trial strain as a starting point for the return mapping, see Section 2. Using the Voigt notation, the strain can be computed from the element unknown $\tilde{\boldsymbol{u}}$ and $\tilde{\boldsymbol{v}}$

$$\begin{aligned}\hat{\boldsymbol{\varepsilon}} &:= \begin{Bmatrix} \varepsilon_{11} \\ \varepsilon_{22} \\ 2\varepsilon_{12} \end{Bmatrix} = \begin{bmatrix} 1 & 0 \\ 0 & 0 \\ 0 & 1 \end{bmatrix} \begin{Bmatrix} \frac{\partial u}{\partial x} \\ \frac{\partial u}{\partial y} \end{Bmatrix} + \begin{bmatrix} 0 & 0 \\ 0 & 1 \\ 1 & 0 \end{bmatrix} \begin{Bmatrix} \frac{\partial v}{\partial x} \\ \frac{\partial v}{\partial y} \end{Bmatrix} \\ &= \boldsymbol{A}_1 \left(\boldsymbol{N}^p\right)^T \boldsymbol{\Pi}^m \tilde{\boldsymbol{u}} + \boldsymbol{A}_2 \left(\boldsymbol{N}^p\right)^T \boldsymbol{\Pi}^m \tilde{\boldsymbol{v}} = \boldsymbol{A} \boldsymbol{N}_p^T \boldsymbol{\Pi}_m \begin{Bmatrix} \tilde{\boldsymbol{u}} \\ \tilde{\boldsymbol{v}} \end{Bmatrix},\end{aligned} \tag{69}$$

where

$$\boldsymbol{A}_1 = \begin{bmatrix} 1 & 0 \\ 0 & 0 \\ 0 & 1 \end{bmatrix}, \boldsymbol{A}_2 = \begin{bmatrix} 0 & 0 \\ 0 & 1 \\ 1 & 0 \end{bmatrix}, \boldsymbol{A} = \begin{bmatrix} \boldsymbol{A}_1 & \boldsymbol{A}_2 \end{bmatrix}, \tag{70}$$

and

$$\boldsymbol{N}_p^T = \begin{bmatrix} \left(\boldsymbol{N}^p\right)^T \\ \left(\boldsymbol{N}^p\right)^T \end{bmatrix}, \quad \boldsymbol{\Pi}_m = \begin{bmatrix} \boldsymbol{\Pi}^m \\ \boldsymbol{\Pi}^m \end{bmatrix}. \tag{71}$$

As discussed in the previous section, elastoplasticity is a history-dependent nonlinear continuous solid mechanical problem. Considering the increment formulation and the strain given in Equation (69), the linearization of the virtual work is obtained from

$$\Delta \mathcal{W} := \int_E \hat{\boldsymbol{\varepsilon}}(\Delta \boldsymbol{u}_h)^T \boldsymbol{C}^{alg} \hat{\boldsymbol{\varepsilon}}(\delta \boldsymbol{v}_h) \mathrm{d}\Omega \tag{72}$$

where $\hat{\boldsymbol{C}}^{alg}$ is the matrix form consistent or algorithmic material tangent (see appendix), which can be determined by the generalized Clark derivative of the nonlinear stress-strain operator $\mathfrak{T}_k(\boldsymbol{\varepsilon}_k)$ as

$$f \leqslant 0 : \boldsymbol{C}^{alg} = \boldsymbol{C}; \tag{73}$$

$$f > 0 : \boldsymbol{C}^{alg} = \boldsymbol{C} - \frac{4\mu^2 \boldsymbol{N} \otimes \boldsymbol{N}}{2\mu + \frac{2}{3}H} - \frac{4\mu^2 \hat{\gamma}}{||\boldsymbol{\eta}_k^{tr}||}(\boldsymbol{I}_{\mathrm{dev}} - \boldsymbol{N} \otimes \boldsymbol{N}), \tag{74}$$

where the plastic consistency parameter $\hat{\gamma}$ as well as the hardening variable and the effective plastic strain can be calculated based on the current stress and strain state. The specific derivation process can be found in the appendix.

Substituting Equations (69) into (72) yields

$$\Delta \mathcal{W} = \begin{Bmatrix} \tilde{\boldsymbol{u}} & \tilde{\boldsymbol{v}} \end{Bmatrix} \boldsymbol{K}_t \begin{Bmatrix} \tilde{\boldsymbol{u}} \\ \tilde{\boldsymbol{v}} \end{Bmatrix} \tag{75}$$

with the tangent matrix in the semi-smooth Newton method can be deduced as

$$\begin{aligned}\boldsymbol{K}_t &= \int_E \boldsymbol{\Pi}_m^T \boldsymbol{N}_p \boldsymbol{A}^T \hat{\boldsymbol{C}}^{alg} \boldsymbol{A} \boldsymbol{N}_p^T \boldsymbol{\Pi}_m \mathrm{d}\Omega \\ &= \boldsymbol{\Pi}_m^T \int_E \boldsymbol{N}_p \boldsymbol{A}^T \hat{\boldsymbol{C}}^{alg} \boldsymbol{A} \boldsymbol{N}_p^T \mathrm{d}\Omega \boldsymbol{\Pi}_m.\end{aligned} \tag{76}$$

The integral in Equation (76) can be calculated by partitioning E into a set of triangles $\mathcal{T}_n$ (as shown in Figure 2) and adopting a Gauss quadrature rule.

The internal force has the form

$$\boldsymbol{F} = \boldsymbol{\Pi}_m^T \int_E \boldsymbol{N}_p \boldsymbol{A}^T \, \hat{\boldsymbol{\sigma}}_k \mathrm{d}\Omega. \tag{77}$$

4.2 | Calculation of stress

In elastoplastic problems, the calculation and updating of stress (strain) is an important part of elastoplastic analysis. Since stress (strain) needs to be calculated at the integration points, considering Equation (69), we have

$$\boldsymbol{\varepsilon}_k^{tr} = \boldsymbol{A}\boldsymbol{N}_p \boldsymbol{\Pi}_m \tilde{\boldsymbol{U}}, \tag{78}$$

where $\tilde{\boldsymbol{U}}$ is the displacement vector and the Voigt notation is assumed for strain. Then the trial stress field can be calculated by

$$\boldsymbol{\sigma}_k^{tr} = (K\mathbf{1} \otimes \mathbf{1} + 2\mu \boldsymbol{I}_{\mathrm{dev}}) : \left(\boldsymbol{\varepsilon}_k^{tr} - \boldsymbol{\varepsilon}_k^{p}\right). \tag{79}$$

If the yield function $f > 0$, the trial stress has to be corrected by

$$\boldsymbol{\sigma}_{k+1} = \boldsymbol{\sigma}_k^{tr} - 2\mu\hat{\gamma}\boldsymbol{N}. \tag{80}$$

5 | NUMERICAL EXAMPLES

This section presents some 2D examples to illustrate the applicability and efficiency of the proposed stabilization-free virtual element method (SFVEM) in solving elastoplastic problems. All computations are performed with self-written Matlab codes. The analysis employs the von Mises yield criterion along with the combined hardening model. Plane strain conditions are assumed. In each example, the polygonal elements are either generated using PolyMesher,[57] or are derived from triangular meshes with subsequent conversion. Two parameters, denoted as k and l, describe the order of the virtual element method and the polynomial order in the L_2 projection operator, respectively.

5.1 | Cook's membrane problem

In this example, the standard Cook's membrane problem is considered. The geometric model, dimensions and boundary conditions are depicted in Figure 13. The structure is clamped at the left side and subjected to a constant distributed vertical load $q_y = 4$ on the right side (as shown in Figure 4). The relevant length specifications are $L = 48$, $H_1 = 44$, and $H_2 = 16$. Perfect plasticity is assumed for this example with the material parameters given as $E = 10000$, $\nu = 0.2$, and $\sigma_Y^0 = 10$.

Two different meshes are selected including a regular mesh and a polygonal mesh (generated by PolyMesher). To compare the performance of the proposed stabilization-free virtual element method, a convergence study is performed for different meshes. By defining the parameter N which corresponds to the number of divisions for each edge, we define four different meshes for regular and polygonal elements. In this example, $N = 2, 3, 4, 5$ is selected leading to $2^N \times 2^N$ elements. The maximum vertical displacement u_y in the y direction of the upper right node is used as a measure in the convergence study.

The selection of parameter l which depends on the number of vertices of element E follows from the relationship between k, l, and n given in the previous section, see Equations (36) and (37). In order to investigate the correct rank of the element matrix, we compare different l for different order k of SFVEM. In this example, we choose $l = 1, 2$ for $k = 1$ and $l = 2, 3$ for $k = 2$. The finite element method with Q1 (linear) element and Q2 (second-order serendipity) element is selected for comparison.

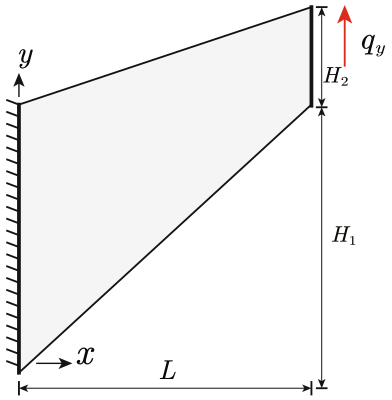

FIGURE 4 Initial configuration of Cook's membrane problem.

TABLE 1 Maximum vertical displacement u_y for different element division N for regular elements (obtained by FEM and SFVEM).

	FEM		SFVEM			
N	Q1	Q2	$k=1, l=1$	$k=1, l=2$	$k=2, l=2$	$k=2, l=3$
2	0.11905	0.17660	0.12008	0.11837	0.18105	0.17857
3	0.15331	0.18273	0.15338	0.15302	0.18469	0.18351
4	0.17323	0.18498	0.17323	0.17317	0.18595	0.18542
5	0.18160	0.18631	0.18159	0.18159	0.18681	0.18651

TABLE 2 Max vertical displacement u_y for different element division N for polygon elements (obtained by SFVEM).

N	$k=1, l=1$	$k=1, l=2$	$k=2, l=2$	$k=2, l=3$
2	0.12762	0.12307	0.18150	0.17943
3	0.14885	0.14565	0.18480	0.18312
4	0.17163	0.17036	0.18628	0.18539
5	0.18097	0.18046	0.18691	0.18651

The values of u_y for different meshes and different methods are given in Tables 1 and 2 for regular and polygonal elements, respectively. Besides, the associated convergence studies for different meshes are depicted in Figures 5 and 6. For regular and polygonal meshes, the solutions obtained by SFVEM agree well with the solutions obtained by FEM. This also indirectly shows that SFVEM is an effective extension of FEM to the polygonal elements.

We note that for $k = 1$, locking occurs when using SFVEM which is due to plastic incompressibility and well known for Q1 FEM element. This could be improved by the use of a mixed formulation, see Reference 25 for incompressibility. For the higher-order SFFEM ($k = 2$), we compared it with the second-order FEM and found that the results were very close. This phenomenon means that locking can be significantly improved by increasing the order of the elements (the locking is not as evident as the first-order SFVEM).

The deformed shape and contour plot of the von Mises stresses for different meshes are shown in Figures 7 and 8.

5.2 | 2D thick cylinder under internal pressure

In this example, a 2D thick-walled cylinder subjected to internal pressure P is considered. The geometrical model, dimensions and boundary conditions are given in Figure 9. The internal diameter is $a = 200$ and the outer diameter is $b = 400$. The inner pressure is selected as $P = 20$. The material parameters are $E = 10000$, $\nu = 0.2$ and perfect plasticity is assumed. The SFVEM with polygonal and regular meshes are used, furthermore, FEM is selected for comparison.

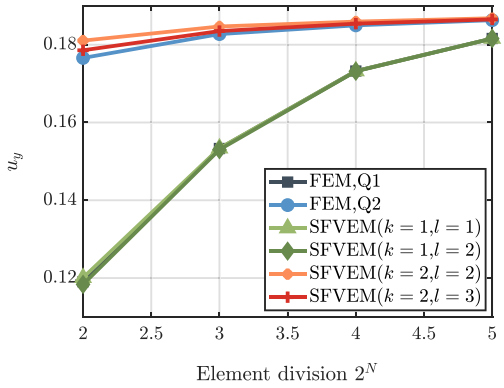

FIGURE 5 Max vertical displacement u_y for different element division N for regular elements.

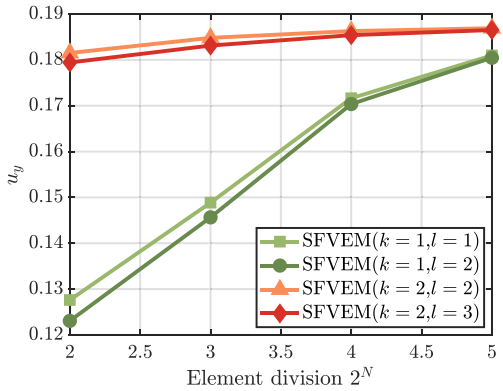

FIGURE 6 Max vertical displacement u_y for different element division N for polygon elements.

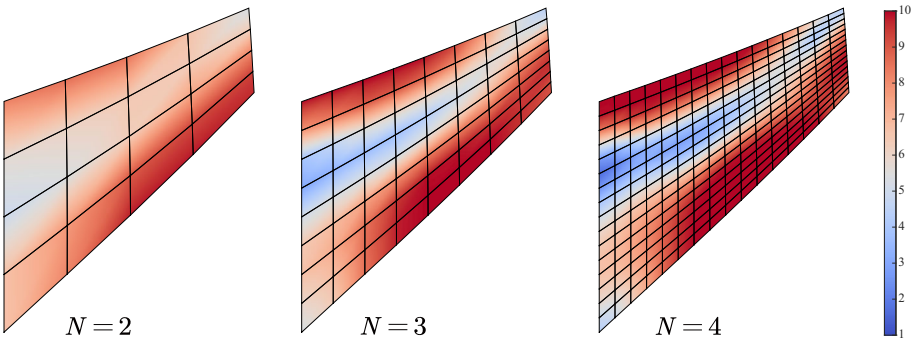

FIGURE 7 Deformed shape and contour plot of the von Mises stresses for different meshes with regular elements (obtained by SFVEM with $k=2, l=3$).

Since this is in reality a 1D axisymmetric problem, an analytical form of its displacement and stress can be deduced. The plastic zone extends from $r=a$ to $r=c$. So the stresses σ_r and σ_θ in the elastic zone $c<r<b$ are given by

$$\sigma_r = \frac{b^2}{b^2-c^2}\left(1-\frac{b^2}{r^2}\right)p_s, c<r<b, \tag{81}$$

$$\sigma_\theta = \frac{c^2}{b^2-c^2}\left(1+\frac{b^2}{r^2}\right)p_s, c<r<b, \tag{82}$$

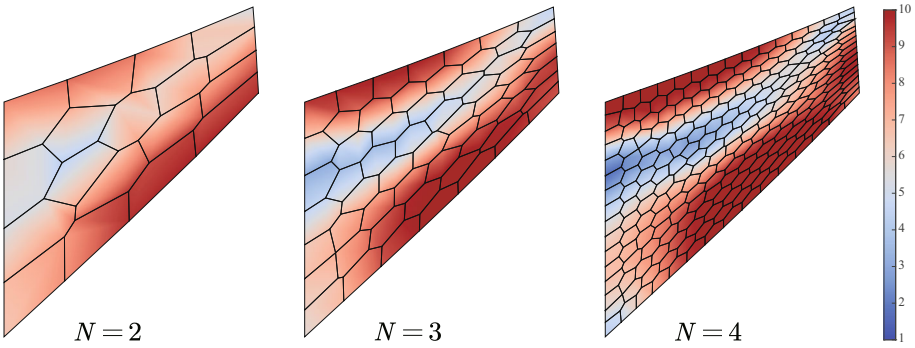

FIGURE 8 Deformed shape and contour plot of the von Mises stresses for different meshes with polygon elements (obtained by SFVEM with $k = 2, l = 3$).

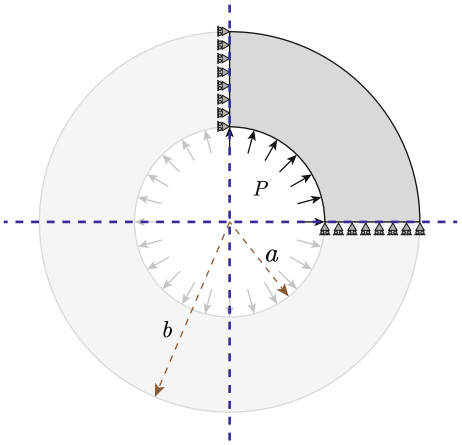

FIGURE 9 Geometry and its dimensions of the 2D thick-walled cylinder.

where

$$p_s = \left(1 - \frac{c^2}{b^2}\right)\frac{\sigma_Y^0}{\sqrt{3}}, \tag{83}$$

and the plastic zone can be determined by

$$p = \frac{2}{3}\sigma_Y^0\left[\ln\frac{c}{a} + \frac{1}{2}\left(1 - \frac{c^2}{b^2}\right)\right]. \tag{84}$$

The stresses in the plastic zone have the form

$$\sigma_r = -P + \frac{2}{\sqrt{3}}\sigma_Y^0 \ln\frac{r}{a}, a < r < c, \tag{85}$$

$$\sigma_\theta = -P + \frac{2}{\sqrt{3}}\sigma_Y^0\left(1 + \ln\frac{r}{a}\right), a < r < c. \tag{86}$$

We assume that the material has different yield stresses $\sigma_Y^0 = 28$ and $\sigma_Y^0 = 30$. For discretizations with $k = 1$ and $k = 2$, the hoop stresses σ_θ along radius for different yield stresses σ_Y^0 obtained by SFVEM and FEM are given in Figures 10 and 11, respectively (polygonal elements are used in SFVEM). The hoop stresses σ_θ obtained by SFVEM coincide well with the solution obtained by FEM and the analytical solutions. We observe a jump in the stress calculation of the finite

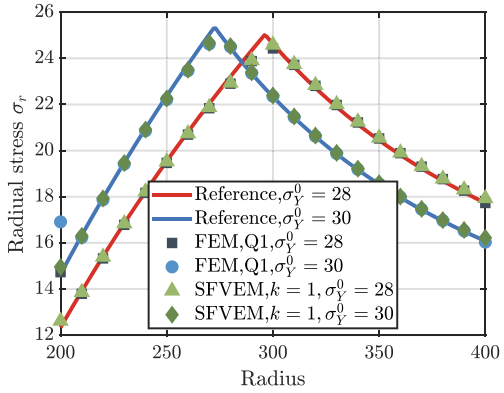

FIGURE 10 Distribution of hoop stresses σ_θ along radius for different yield stresses σ_Y^0 (first order).

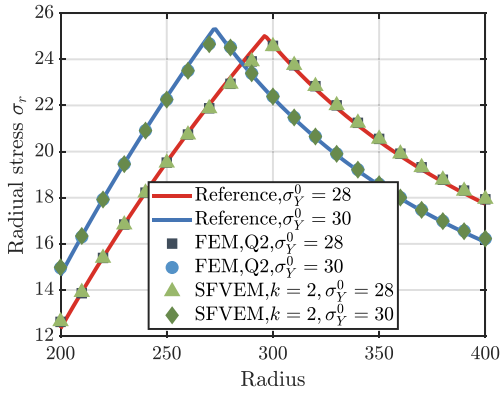

FIGURE 11 Distribution of hoop stresses σ_θ along radius for different yield stresses σ_Y^0 (second order).

TABLE 3 Max vertical displacement u_y for different element division N for polygon elements.

	Analytical	FEM, Q1	FEM, Q2	SFVEM, $k = 1, l = 2$	SFVEM, $k = 2, l = 3$
$\sigma_Y^0 = 28$	25.007	24.429	24.794	24.583	24.563
$\sigma_Y^0 = 30$	25.303	24.619	25.059	24.693	24.855

element method at $r = a$ but there is no such phenomenon in SFVEM for the first-order method ($k = 1$). This may be due to inaccurate interpolation of nodal stresses.

The maximum values of σ_y are compared and listed in Table 3 for different methods. It can be seen that the stress results obtained by SFVEM are in good agreement with the reference solutions as given in Table 3.

The contour plots of the von Mises stress for different yield stresses obtained by SFVEM are shown in Figure 12.

5.3 | Elastoplastic problem with loading-unloading

An angle plate is subjected to a time-varying load cycle. The geometric model, dimensions and boundary conditions are provided in Figure 13. Von Mises plasticity with kinematic hardening is considered with the material parameters $E = 206900$, $\nu = 0.29$, $\sigma_Y^0 = 450$, and $H = 20000$. The time-varying traction force $F(t)$ depicted in Figure 14 is applied on the top of the model. The maximum load is $F_{\max} = 200$.

SFVEM and FEM are selected for the numerical simulation. The parameters used in SFVEM are chosen as $l = 2$ for $k = 1$ and $l = 3$ for $k = 2$. In fact, $l = 1$ for $k = 1$ and $l = 2$ for $k = 2$ are also acceptable in this example since the maximum

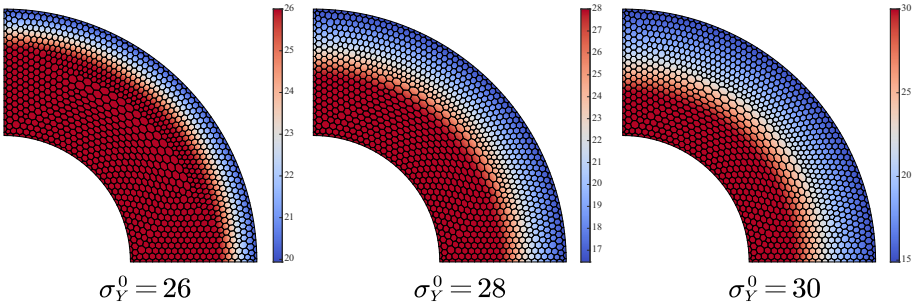

FIGURE 12 Contour plot of the von Mises stresses for different yield stress σ_Y^0 with polygon elements (obtained by SFVEM with $k = 2, l = 3$).

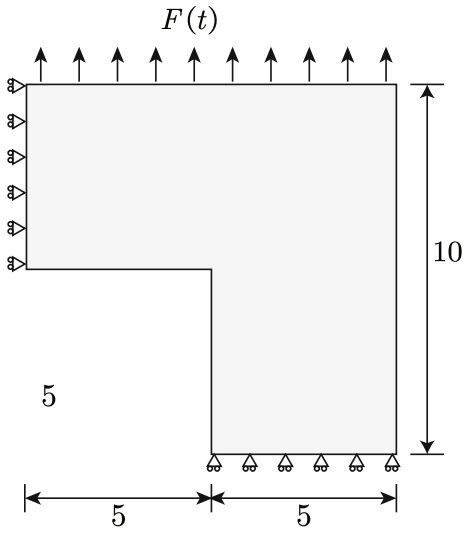

FIGURE 13 Geometry and its dimensions of the 2D plane.

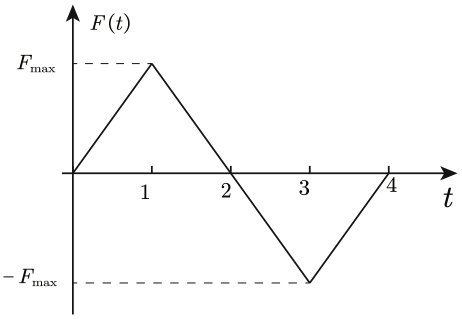

FIGURE 14 History of the traction force.

number of nodes in an element is $n = 6$. The polygonal mesh is constructed from triangular elements. The contour plots of von Mises stress obtained by SFVEM and FEM methods are given in Figures 15 and 16 for $t = 1$ and $t = 4$, respectively.

We further study the relationship between the loading scale $0 \leqslant \tau \leqslant 4$ and the work of the external force (hysteresis phenomenon of plastic materials). For different methods and different parameters, the relation between τ and the work of the external force is depicted in Figure 17. We note that there are some differences in the results obtained by the finite element method of first and second order, which is related to the locking of Q1 elements. The results obtained by SFVEM

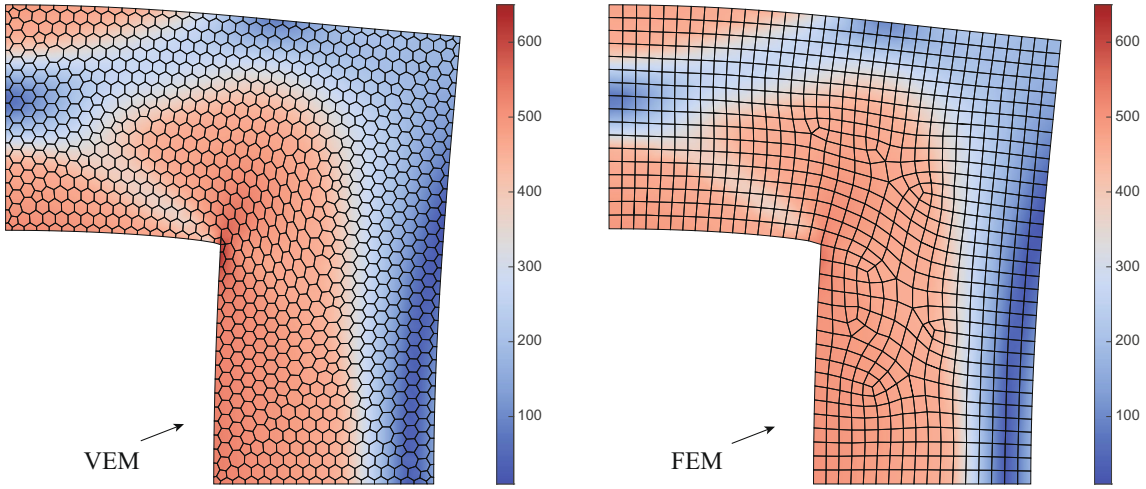

FIGURE 15 Contour plot of von Mises stress with the deformed shape at $t = 1.0$, Q1 elements are used in FEM and the parameters in VEM are selected as $k = 1$ and $l = 2$.

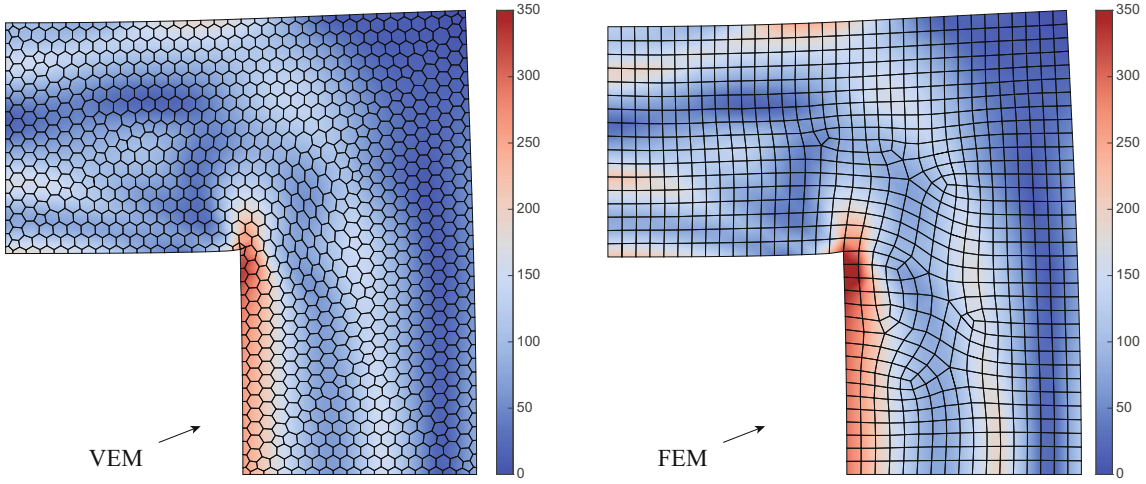

FIGURE 16 Contour plot of von Mises stress with the deformed shape at $t = 4.0$, Q1 elements are used in FEM and the parameters in VEM are selected as $k = 1$ and $l = 2$.

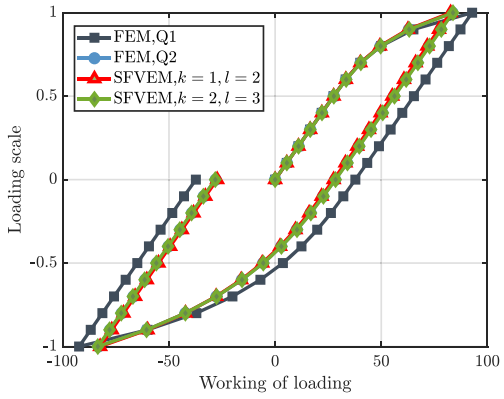

FIGURE 17 The hysteresis curve for different methods.

TABLE 4 Values of work obtained by different methods.

t	FEM, Q1	FEM, Q2	SFVEM $k=1, l=2$	SFVEM $k=2, l=3$
1	92.80	83.52	82.68	83.79
2	37.79	28.27	27.56	28.46
3	−92.34	−83.26	−82.43	−83.52
4	−37.33	−28.01	−27.30	−28.19

attach well with the results obtained by second-order FEM, even for first-order SFVEM. This underlines for this example that SFVEM is less prone to locking for $k = 1$.

The values obtained by different methods at $t = 1$, $t = 2$, $t = 3$, and $t = 4$ are displayed in Table 4. Compared to the Q1 finite element, the results of SFVEM ($k = 1$) are more consistent with those of the second-order finite element method.

6 | CONCLUSION

In this paper, we extend the application of the stabilization-free virtual element method (SFVEM) to 2D elastoplastic problems. Higher-order L_2 projections of the enhanced gradient denoted as $\mathbf{\Pi}^m$ are introduced alongside the $\mathbf{\Pi}^\nabla$ projector used in conventional VEM. Under appropriate selection of the enhanced polynomial space, a coercive bilinear form can be established which results in a stiffness matrix that has the correct rank and encompasses the physical zero-energy modes. In the calculation process of SFVEM, no additional stability terms are required, making the method very similar to traditional finite element methods. Based on the framework mentioned above, we provide a stabilization-free virtual element method for solving classical elastoplastic mechanical problems which is used for the computational analysis of some classical problems. Both first-order and second-order SFVEMs perform well in this nonlinear elastoplastic problem.

ACKNOWLEDGMENTS

The first and last authors are grateful for the support provided by the Alexander von Humboldt Foundation. Open Access funding enabled and organized by Projekt DEAL.

CONFLICT OF INTEREST STATEMENT

The authors declare no potential conflict of interest.

DATA AVAILABILITY STATEMENT

The data that support the findings of this study are available from the corresponding author upon reasonable request.

REFERENCES

1. Cottrell JA, Hughes TJ, Bazilevs Y. *Isogeometric Analysis: Toward Integration of CAD and FEA*. John Wiley & Sons; 2009.
2. Sukumar N, Tabarraei A. Conformal polygonal finite elements. *Int J Numer Methods Eng*. 2004;61:2045-2066. doi:10.1002/nme.1141
3. Nguyen-Xuan H. A polygonal finite element method for plate analysis. *Comput Struct*. 2017;188:45-62. doi:10.1016/j.compstruc.2017.04.002
4. Di Pietro DA, Ern A. *Mathematical Aspects of Discontinuous Galerkin Methods*. Springer; 2012.
5. Hesthaven J, Warburton T. *Nodal Discontinuous Galerkin Methods: Algorithms, Analysis, and Applications*. Vol 54. Springer; 2007.
6. Veiga L, Lipnikov K, Manzini G. *The Mimetic Finite Difference Method for Elliptic Problems*. Springer Cham; 2014.
7. Brezzi F, Lipnikov K, Simoncini V. A family of mimetic finite difference methods on polygonal and polyhedral meshes. *Math Models Methods Appl Sci*. 2005;15:1533-1551. doi:10.1142/S0218202505000832
8. Tishkin V, Samarskii A, Favorskii A, Shashkov M. Operational finite-difference schemes. *Differ Equ*. 1981;17:854-862.
9. Moes N, Dolbow J, Belytschko T. A finite element method for crack growth without Remeshing. *Int J Numer Methods Eng*. 1999;46:131-150. doi:10.1002/(SICI)1097-0207(19990910)46:13.0.CO;2-J
10. Strouboulis T, Babuška I, Copps K. The design and analysis of the generalized finite element method. *Comput Methods Appl Mech Eng*. 2000;181:43-69. doi:10.1016/S0045-7825(99)00072-9
11. Song C. The Scaled Boundary Finite Element Method: Introduction to Theory and Implementation. 2018.
12. Xiao B, Natarajan S, Birk C, Ooi E, Song C, Ooi ET. Construction of generalized shape functions over arbitrary polytopes based on scaled boundary finite element method's solution of Poisson's equation. *Int J Numer Methods Eng*. 2023;124(17):3603-3636. doi:10.1002/nme.7287

13. Ooi ET, Song C, Natarajan S. A scaled boundary finite element formulation with bubble functions for Elasto-static analyses of functionally graded materials. *Comput Mech*. 2017;60:943-967. doi:10.1007/s00466-017-1443-y
14. Veiga L, Brezzi F, Cangiani A, Manzini G, Marini L, Russo A. Basic principles of virtual element methods. *Math Models Methods Appl Sci*. 2012;23:199-214. doi:10.1142/S0218202512500492
15. Veiga L, Brezzi F, Marini L, Russo A. Mixed virtual element methods for general second order elliptic problems on polygonal meshes. *ESAIM Math Model Numer Anal*. 2014;26:727-747. doi:10.1051/m2an/2015067
16. Artioli E, Veiga L, Lovadina C, Sacco E. Arbitrary order 2D virtual elements for polygonal meshes: part I, elastic problem. *Comput Mech*. 2017;60:727-747. doi:10.1007/s00466-017-1404-5
17. Nguyen-Thanh VM, Zhuang X, Nguyen-Xuan H, Rabczuk T, Wriggers P. A virtual element method for 2D linear elastic fracture analysis. *Comput Methods Appl Mech Eng*. 2018;340:366-395. doi:10.1016/j.cma.2018.05.021
18. Hussein A, Aldakheel F, Hudobivnik B, Wriggers P, Guidault PA, Allix O. A computational framework for brittle crack-propagation based on efficient virtual element method. *Finite Elem Anal Des*. 2019;159:15-32. doi:10.1016/j.finel.2019.03.001
19. Huyssteen vD, Lopez Rivarola F, Etse G, Steinmann P. On mesh refinement procedures for the virtual element method for two-dimensional elastic problems. *Comput Methods Appl Mech Eng*. 2022;393:114849. doi:10.1016/j.cma.2022.114849
20. Veiga L, Brezzi F. Virtual elements for linear elasticity problems. *SIAM J Numer Anal*. 2013;51(2):794-812. doi:10.1137/120874746
21. Gain A, Talischi C, Paulino G. On the virtual element method for three-dimensional elasticity problems on arbitrary polyhedral meshes. *Comput Methods Appl Mech Eng*. 2013;282:132-160. doi:10.1016/j.cma.2014.05.005
22. Dassi F, Lovadina C, Visinoni M. A three-dimensional Hellinger-Reissner virtual element method for linear elasticity problems. *Comput Methods Appl Mech Eng*. 2020;364:112910. doi:10.1016/j.cma.2020.112910
23. Mengolini M, Benedetto M, Aragón A. An engineering perspective to the virtual element method and its interplay with the standard finite element method. *Comput Methods Appl Mech Eng*. 2019;350:995-1023. doi:10.1016/j.cma.2019.02.043
24. Chi H, Veiga L, Paulino G. Some basic formulations of the virtual element method (VEM) for finite deformations. *Comput Methods Appl Mech Eng*. 2016;318:995-1023. doi:10.1016/j.cma.2016.12.020
25. Wriggers P, Reddy B, Rust W, Hudobivnik B. Efficient virtual element formulations for compressible and incompressible finite deformations. *Comput Mech*. 2017;60:995-1023. doi:10.1007/s00466-017-1405-4
26. Huyssteen D, Reddy B. A virtual element method for isotropic hyperelasticity. *Comput Methods Appl Mech Eng*. 2020;367:113134. doi:10.1016/j.cma.2020.113134
27. De Bellis M, Wriggers P, Hudobivnik B. Serendipity virtual element formulation for nonlinear elasticity. *Comput Struct*. 2019;223:106094. doi:10.1016/j.compstruc.2019.07.003
28. Wriggers P, Rust W, Reddy B. A virtual element method for contact. *Comput Mech*. 2016;58:995-1023. doi:10.1007/s00466-016-1331-x
29. Aldakheel F, Hudobivnik B, Artioli E, Veiga L, Wriggers P. Curvilinear virtual elements for contact mechanics. *Comput Methods Appl Mech Eng*. 2020;372:113394. doi:10.1016/j.cma.2020.113394
30. Shen W, Ohsaki M, Zhang J. A 2-dimentional contact analysis using second-order virtual element method. *Comput Mech*. 2022;70:995-1023. doi:10.1007/s00466-022-02165-y
31. Cihan M, Hudobivnik B, Korelc J, Wriggers P. A virtual element method for 3D contact problems with non-conforming meshes. *Comput Methods Appl Mech Eng*. 2022;402:115385. doi:10.1016/j.cma.2022.115385
32. Park K, Chi H, Paulino G. On nonconvex meshes for elastodynamics using virtual element methods with explicit time integration. *Comput Methods Appl Mech Eng*. 2019;356:669-684. doi:10.1016/j.cma.2019.06.031
33. Park K, Chi H, Paulino G. Numerical recipes for elastodynamic virtual element methods with explicit time integration. *Int J Numer Methods Eng*. 2019;121:1-31. doi:10.1002/nme.6173
34. Cihan M, Hudobivnik B, Aldakheel F, Wriggers P. Virtual element formulation for finite strain elastodynamics. *Comput Model Eng Sci*. 2021;129:1151-1180. doi:10.32604/cmes.2021.016851
35. Sukumar N, Tupek M. Virtual elements on agglomerated finite elements to increase the critical time step in elastodynamic simulations. *Int J Numer Methods Eng*. 2022;123:4702-4725. doi:10.1002/nme.7052
36. Wriggers P, Hudobivnik B. A low order virtual element formulation for finite elasto-plastic deformations. *Comput Methods Appl Mech Eng*. 2017;327:4702-4725. doi:10.1016/j.cma.2017.08.053
37. Hudobivnik B, Aldakheel F, Wriggers P. A low order 3D virtual element formulation for finite elasto–plastic deformations. *Comput Mech*. 2019;63:4702-4725. doi:10.1007/s00466-018-1593-6
38. Cihan M, Hudobivnik B, Aldakheel F, Wriggers P. 3D mixed virtual element formulation for dynamic elasto-plastic analysis. *Comput Mech*. 2021;68:1-18. doi:10.1007/s00466-021-02010-8
39. Liu TR, Aldakheel F, Aliabadi M. Virtual element method for phase field modeling of dynamic fracture. *Comput Methods Appl Mech Eng*. 2023;411:116050. doi:10.1016/j.cma.2023.116050
40. Aldakheel F, Hudobivnik B, Wriggers P. Virtual element formulation for phase-field modeling of ductile fracture. *Int J Multiscale Comput Eng*. 2019;17:181-200. doi:10.1615/IntJMultCompEng.2018026804
41. Certik O, Gardini F, Manzini G, Mascotto L, Vacca G. The p - and h p -versions of the virtual element method for elliptic eigenvalue problems. *Comput Math Appl*. 2019;79:4702-4725. doi:10.1016/j.camwa.2019.10.018
42. Meng J, Wang G, Mei L. Mixed virtual element method for the Helmholtz transmission eigenvalue problem on polytopal meshes. *IMA J Numer Anal*. 2022;43:4702-4725. doi:10.1093/imanum/drac019
43. Lamperti A, Cremonesi M, Perego U, Russo A, Lovadina C. A Hu-Washizu variational approach to self-stabilized virtual elements: 2D linear elastostatics. *Comput Mech*. 2023;71:1-21. doi:10.1007/s00466-023-02282-2

44. D'Altri A, Miranda S, Patruno L, Sacco E. An enhanced VEM formulation for plane elasticity. *Comput Methods Appl Mech Eng*. 2021;376:113663. doi:10.1016/j.cma.2020.113663
45. Berrone S, Borio A, Marcon F, Teora G. A first-order stabilization-free virtual element method. *Appl Math Lett*. 2023;142:108641. doi:10.1016/j.aml.2023.108641
46. Berrone S, Borio A, Marcon F. Lowest order stabilization free Virtual Element Method for the Poisson equation. arXiv preprint:2103.16896 2021.
47. Chen A, Sukumar N. Stabilization-free virtual element method for plane elasticity. *Comput Math Appl*. 2023;138:88-105. doi:10.1016/j.camwa.2023.03.002
48. Berrone S, Borio A, Marcon F. Comparison of standard and stabilization free virtual elements on anisotropic elliptic problems. *Appl Math Lett*. 2022;129:107971. doi:10.1016/j.aml.2022.107971
49. Meng J, Wang X, Bu L, Mei L. A lowest-order free-stabilization virtual element method for the Laplacian eigenvalue problem. *J Comput Appl Math*. 2022;410:114013. doi:10.1016/j.cam.2021.114013
50. Chen A, Sukumar N. Stabilization-free serendipity virtual element method for plane elasticity. *Comput Methods Appl Mech Eng*. 2023;404:115784. doi:10.1016/j.cma.2022.115784
51. Xu BB, Wriggers P. 3D stabilization-free virtual element method for linear elastic analysis. *Comput Methods Appl Mech Eng*. 2024;421:116826. doi:10.1016/j.cma.2024.116826
52. Xu BB, Peng F, Wriggers P. Stabilization-free virtual element method for finite strain applications. *Comput Methods Appl Mech Eng*. 2023;417:116555. doi:10.1016/j.cma.2023.116555
53. Wriggers P. *Nonlinear Finite Element Methods*. Springer Verlag; 2008.
54. Veiga B dL, Lovadina C, Russo A. Stability analysis for the virtual element method. *Math Models Methods Appl Sci*. 2016;27:2557-2594. doi:10.1142/S021820251750052X
55. Cangiani A, Manzini G, Sutton O. Conforming and nonconforming virtual element methods for elliptic problems. *J Numer Anal*. 2015;37:1317-1354. doi:10.1093/imanum/drw036
56. Ahmad B, Alsaedi A, Brezzi F, Marini L, Russo A. Equivalent projectors for virtual element methods. *Comput Math Appl*. 2013;66:376-391. doi:10.1016/j.camwa.2013.05.015
57. Talischi C, Paulino G, Pereira A, Menezes I. PolyMesher: a general-purpose mesh generator for polygonal elements written in MATLAB. *Struct Multidiscip Optim*. 2012;45:309-328. doi:10.1007/s00158-011-0706-z
58. Sysala S. Properties and simplifications of constitutive time-discretized elastoplastic operators. *ZAMM - J Appl Math Mech / Zeitschrift Fur Angewandte Mathematik Und Mechanik*. 2014;94:233-255. doi:10.1002/zamm.201200056
59. Cermak M, Sysala S, Valdman J. Efficient and flexible MATLAB implementation of 2D and 3D elastoplastic problems. *Appl Math Comput*. 2018;355:595-614. doi:10.1016/J.AMC.2019.02.054

How to cite this article: Xu B-B, Wang Y-F, Wriggers P. Stabilization-free virtual element method for 2D elastoplastic problems. *Int J Numer Methods Eng*. 2024;e7490. doi: 10.1002/nme.7490

APPENDIX A. TIME DISCRETIZATION SCHEME OF THE CONSTITUTIVE PROBLEM

We have discussed the elastoplastic equation in Section 2. Since constitutive relations and evolution of plastic variables are in the form of rates, the (pseudo) time step should be selected. Consider a discretization of time interval $[0 = t_0 < t_1 < \cdots < t_k < \cdots < t_N = t_{\max}]$ and denote $\boldsymbol{\sigma}_k := \boldsymbol{\sigma}(t_k), \boldsymbol{\varepsilon}_k := \boldsymbol{\varepsilon}(t_k), \boldsymbol{s}_k := \boldsymbol{s}(t_k), \boldsymbol{q}_k := \boldsymbol{q}(t_k), \boldsymbol{\eta}_k := \boldsymbol{\eta}(t_k)$, the kth step of the incremental constitutive problem discretized by the implicit backward scheme based on the Karush-Kuhn-Tucker (KKT) condition. In this work, only linear isotropic and kinematic hardening are considered, so the process of nonlinear analysis is simplified.

Besides, we can define the nonlinear (piecewise linear) stress-strain operator $\mathfrak{T}_k$ at time t_k as

$$\boldsymbol{\sigma}_k = \mathfrak{T}_k(\boldsymbol{\varepsilon}_k). \tag{A1}$$

In general, the stress-strain operator $\mathfrak{T}_k$ is implicit and the elastic predictor–plastic corrector method can be applied. The idea of this procedure is to freeze the plastic variables at the beginning of a time step from t_k to t_{k+1}:

$$\boldsymbol{s}_{k+1}^{tr} = \boldsymbol{s}_k, \quad \left(\boldsymbol{\varepsilon}_{k+1}^{p}\right)^{tr} = \boldsymbol{\varepsilon}_k^{p}, \quad \boldsymbol{\alpha}_{k+1}^{tr} = \boldsymbol{\alpha}_k. \tag{A2}$$

where $(\bullet)^{tr}$ denotes the trial status.

Then within the elastic prediction, we should check whether the trial stress is admissible or not. If $f \leq 0$, the trial stress is within the elastic domain, then

$$\left(\boldsymbol{\varepsilon}_{k+1}^{p}\right)^{tr} = \boldsymbol{\varepsilon}_{k}^{p}, \quad \boldsymbol{\alpha}_{k+1}^{tr} = \boldsymbol{\alpha}_{k}. \tag{A3}$$

If the trial stress is outside the elastic domain, that is, $f > 0$, the plastic correction step needs to be carried out and the trial stress has the form as

$$\boldsymbol{s}_{k+1} = \boldsymbol{s}_{k}^{tr} - 2\mu\Delta\boldsymbol{\varepsilon}^{p} = \boldsymbol{s}_{k}^{tr} - 2\mu\hat{\gamma}\boldsymbol{N}, \tag{A4}$$

where $\hat{\gamma} = \Delta t\lambda$ and $\boldsymbol{N} = \boldsymbol{\eta}_{k}^{tr}/||\boldsymbol{\eta}_{k}^{tr}||$. Rather, the stress itself can be updated by

$$\boldsymbol{\sigma}_{k+1} = \boldsymbol{\sigma}_{k} + \Delta\boldsymbol{\sigma} \tag{A5}$$

where $\Delta\boldsymbol{\sigma} = \boldsymbol{C}\Delta\boldsymbol{\varepsilon} - 2\mu\hat{\gamma}\boldsymbol{N}$. The plastic variables are also updated with the stress according to the flow rule as

$$\boldsymbol{q}_{k+1} = \boldsymbol{q}_{k}^{tr} + \frac{2}{3}H\hat{\gamma}\boldsymbol{N}, \quad \hat{\alpha}_{k+1} = \hat{\alpha}_{k} + \sqrt{\frac{2}{3}}\hat{\gamma} \tag{A6}$$

As given in References 58,59, the nonlinear stress-strain operator $\mathfrak{T}_{k}$ is almost everywhere differentiable and can define a function

$$\mathfrak{T}_{k}^{0} : \mathbb{R}_{sym}^{3\times3} \rightarrow \mathcal{L}\left(\mathbb{R}_{sym}^{3\times3} \times \mathbb{R}_{sym}^{3\times3}\right) \tag{A7}$$

representing a generalized Clark derivative of $\mathfrak{T}_{k}$. In elastic cases, the stress-strain operator and its derivative have the form as

$$\mathfrak{T}_{k}(\boldsymbol{\varepsilon}_{k}) = \boldsymbol{C} : \boldsymbol{\varepsilon}_{k}, \quad \mathfrak{T}_{k}^{0}(\boldsymbol{\varepsilon}_{k}) = \boldsymbol{C}, \tag{A8}$$

where the elastic constitutive tensor $\boldsymbol{C}$ is given in Equation (7). In the plastic cases, we have

$$\mathfrak{T}_{k}^{0}(\boldsymbol{\varepsilon}_{k}) = \boldsymbol{C}^{alg} = \boldsymbol{C} - \frac{4\mu^{2}\boldsymbol{N}\otimes\boldsymbol{N}}{2\mu + \frac{2}{3}H} - \frac{4\mu^{2}\hat{\gamma}}{||\boldsymbol{\eta}_{k}^{tr}||}(\boldsymbol{I}_{\text{dev}} - \boldsymbol{N}\otimes\boldsymbol{N}). \tag{A9}$$

Besides, the stress-strain operator has the form as

$$\mathfrak{T}_{k}(\boldsymbol{\varepsilon}_{k}) = \boldsymbol{\sigma}_{k}^{tr} - 2\mu\hat{\gamma}\boldsymbol{N}. \tag{A10}$$